Journal of Materials Chemistry A

Mechanical Properties of a Gallium Fumarate Metal-Organic Framework: A Joint Experimental-Modelling Exploration

Journal:	*Journal of Materials Chemistry A*
Manuscript ID	TA-ART-02-2017-001559.R2
Article Type:	Paper
Date Submitted by the Author:	07-May-2017

Complete List of Authors:	Ramaswamy, Padmini; Kyoto University, Wieme, Jelle; Ghent University, Center for molecular modeling CMM Alvarez, Elsa; Université de Versailles St-Quentin, Institut Lavoisier Versailles Vanduyfhuys, Louis; Ghent University, Center For Molecular Modeling Itié, Jean-Paul; Synchrotron Soleil, Fabry, Paul; University of Versailles. Institut Lavoisier , Van Speybroeck, Veronique; Ghent University, Center For Molecular Modeling Serre, Christian; Université de Versailles St Quentin en Yvelines, Institut Lavoisier, UMR CNRS 8180 Yot, Pascal G.; University of Montpellier, Institut Charles Gerhardt Montpellier Maurin, Guillaume; Université de Montpellier II, Institut Charles Gerhardt

Journal of Material Chemistry A

ARTICLE

Mechanical Properties of a Gallium Fumarate Metal-Organic Framework: A Joint Experimental-Modelling Exploration

Received 00th January 20xx,
Accepted 00th January 20xx

DOI: 10.1039/x0xx00000x

www.rsc.org/

Padmini Ramaswamy,[a] Jelle Wieme,[b] Elsa Alvarez,[c,] Louis Vanduyfhuys,[b] Jean-Paul Itié,[d] Paul Fabry,[c] Veronique Van Speybroeck,[b] Christian Serre,[e] Pascal. G. Yot,*[a] Guillaume Maurin,[a]

A gallium analogue of the commercially available Al-fumarate MOF A520 - recently identified as isotypic to MIL-53(Al)-BDC - has been synthesized for the first time and further characterized in its hydrated and dehydrated forms. The structural response under applied mechanical pressure of this MIL-53(Ga)-FA solid was investigated using advanced experimental techniques coupled with computational tools. Hg porosimetry and high-pressure X-Ray Powder Diffraction (XRPD) experiments evidenced that the pristine dehydrated large pore form undergoes an irreversible structure contraction upon an applied pressure of 85 MPa with an associated volume change of ~14% which makes this material promising for mechanical energy storage applications, in particular as a shock absorber. The breathing behavior was further rationalized by performing a series of periodic Density Functional Theory (DFT) calculations with the construction of an energy profile as a function of volume for both MIL-53(Ga)-FA and its aluminium analogue. As such we unravelled the microscopic origin of the difference in pressure-induced behavior for the aluminium and gallium fumarate based materials.

1. Introduction

Metal-Organic Frameworks (MOFs) are a versatile class of porous crystalline hybrid materials consisting of metal ions bridged by organic ligands.[1,2] This family of porous solids is especially of interest due to the wide spectrum of materials that can be prepared. Almost all the elements of the periodic table and a large variety of organic linkers have been used in one structure or another, leading to materials with a huge variety of physical properties. MOFs have hitherto been envisaged for a large number of applications such as gas storage and gas/liquid separation,[3-11] adsorption-based heat-pump[12], biomedicine,[13,14] catalysis,[15,16,17,18] photoluminescence,[19,20] magnetism,[21,22] proton conductivity[23,24] etc. However, the thermo-mechanical properties of MOFs and their potential related-applications have been less explored so far.[25-39] One of the early reports in literature by Chapman *et al*. focused on the study of the effect of the size and penetrability of guest molecules on the compressibility of CuBTC or HKUST-1.[26] Later, the pressure-induced structure behaviour of ZIFs was investigated.[27-29] More recently, MIL-53(Al) and its amino-functionalized form were explored under applied pressure by Serra-Crespo *et al*., and this study revealed a negative linear compressibility in these solids.[30] Other studies focused on the pressure-induced amorphization of a series of MOFs in a wide range of applied pressures, from 6.5 GPa for ZIF-4[33] to 3.5 MPa for MOF-5,[31] and 1.8 GPa for UiO-66[32,40,41]. Most of these experiments have been performed by *in situ* high-pressure X-ray or neutron powder diffraction based on the use of diamond anvil cells and a non-penetrating inert fluid to ensure hydrostatic compression of the solids. With regard to potential applications, several members of the highly flexible MIL-53 series have been shown to possess structural features that render them attractive for use in energy absorption/storage related-applications such as dampers and shock absorbers.[34-38] In this context, some of us recently reported the optimized synthesis and structural characterization of the commercially available aluminium fumarate A520.[42] We showed that this solid exhibits a structure strongly related to the MIL-53 topology and thus was labelled as MIL-53(Al)-FA. This material undergoes a reversible structural contraction which can be controlled by the application of an external pressure, resulting in unprecedented values for work and heat energies, thereby showing great promises for mechanical storage applications.[37] MIL-53(Al)-FA was also found to exhibit interesting heat transfer reallocation properties that could have potential interests for thermally-driven adsorption chillers or heat-

[a] *Institut Charles Gerhardt Montpellier UMR 5253 CNRS UM ENSCM, Université de Montpellier, CC 15005, Place Eugène Bataillon, F-34095 Montpellier cedex 05, France. *e-mail: pascal.yot@umontpellier.fr; Tel.: +33 4 67 14 32 94; Fax: +33 4 67 14 42 90.*
[b] *Centre for Molecular Modeling, Ghent University, Technologiepark 903, B-9052 Zwijnaarde, Belgium. Centre for Molecular Modeling, Ghent University, Technologie park 903, B-9052 Zwijnaarde, Belgium.*
[c] *Institut Lavoisier Versailles, Université de Versailles St-Quentin, 45, avenue des Etats-Unis, F-78035 Versailles cedex, France, Université Paris Saclay (France).*
[d] *Synchrotron Soleil, L'orme des Merisiers, Saint-Aubin - BP 48, F-91192 Gif-sur-Yvette cedex, France.*
[e] *Institut des Matériaux Poreux de Paris (IMAP), FRE CNRS 2000, Ecole Normale Supérieure de Paris, Ecole Supérieure de Physique et de Chimie Industrielles de Paris, PSL Research University, 75005 Paris (France)*
Electronic Supplementary Information (ESI) available: Experimental procedures, X-ray diffraction, and molecular simulation. See DOI: 10.1039/x0xx00000x

pumps. [43] In this latter application, one point of attention is the material's mechanical stability under the influence of capillary forces during successive adsorption/desorption cycles, which needs to be ensured.[43]

In light of the diverse range of technologically relevant properties exhibited by this aluminium-fumarate MOF, we decided to expand our investigations into the series of MIL-53-fumarate with various metal cations. Previous studies on the related highly flexible MIL-53-BDC (Al, Cr, Fe, Ga, Sc, BDC=1, 4-benzene dicarboxylate) frameworks have demonstrated that the metal center plays a very crucial role in tuning the magnitude of the flexibility of this family of materials, not only upon adsorption, but also under thermal and mechanical stimuli, leading to strong differences in terms of energy storage as well as reversible or irreversible structural switching behaviours.[34-36,44-50] Herein we report our results on the gallium fumarate, denoted MIL-53(Ga)-FA, whose characterizations are strongly in favour of an isoreticular character between this solid and the MIL-53(Al)-FA MOF. Hg-porosimetry and *in-situ* high-pressure synchrotron X-ray diffraction were combined with advanced periodic Density Functional Theory (DFT) calculations to study the structural changes of this flexible solid under applied moderate pressures up to 2 GPa. This joint experimental-computational approach allowed the determination of the transition pressure and the magnitude of the volume change related to the structural switching of MIL-53(Ga)-FA towards a more contracted phase. Finally, the reversibility of the structural transition was explored for potential applications of this solid to the field of mechanical energy storage. As anticipated by similar studies performed on the MIL-53-BDC frameworks, the nature of the metal center impacts the pressure-induced behaviour of the fumarate-based materials and the origin has been revealed by the DFT calculations.

2. Material and methods

2.1. Synthesis and characterisations

MIL-53(Ga)-FA was prepared from a reaction mixture of composition Ga(III) nitrate ($Ga^{III}(NO_3)_3(H_2O)_x$): fumaric acid: water: NaOH=1:0.5:275:1, which was heated at 403 K in a Teflon-lined autoclave for 10 hours with a ramped heating rate of 7 $K.min^{-1}$. The solid was recovered by filtration and washed with water and ethanol. In the Infra-Red (IR) spectrum of MIL-53(Ga)-FAas (as for as-synthesized), a band at about 1710 cm^{-1}, characteristic of the ν(C=O) mode of the carboxyl groups of residual traces of the free fumaric acid was observed (Figure S1, Supporting Information). This band subsequently disappears with successive washings, indicating the full departure of the entrapped or recrystallized fumaric acid. The thermogravimetric analysis (Figure S2) shows two different weight losses at 360 and 460 K corresponding to the loss of water and linker respectively. This is consistent with the proposed formula, Ga(OH)(fum) (fum for fumarate), the difference possibly arising from an excess of metal oxide or linker defects (experimental: 54 % vs. theoretical: 47 %), similar to that observed previously in the synthesis of the aluminium fumarate solid.[37] MIL-53(Ga)-FA reveals at first sight a I-type N_2 adsorption isotherm characteristic for microporous solids (Figure S3). The corresponding BET area is 750(20) $m^2.g^{-1}$ slightly lower than the value previously reported for the Al-fumarate phase, partially due to the higher crystal density of this solid.[42] The X-ray powder diffraction pattern of MIL-53(Ga)-FA is very close to the one of MIL-53(Al)-FA, associated with a slight shift of the main diffraction Bragg peaks to low angle in agreement with a larger ionic radius of Ga^{3+} compared to Al^{3+} (Figure 1). Further experimental details are provided in the Supporting Information.

2.2. Mercury Intrusion

Mercury intrusion experiments were carried out to characterize the pressure-induced structural response of the dehydrated solid with a Micromeritics Autopore 9240 porosimeter. Prior to intrusion, the sample was first activated at 383 K under secondary vacuum for 8 hours. Two intrusion–extrusion (compression–decompression) cycles were applied to the samples in the pressure range 10^{-4} to 420 MPa (see Supporting Information).

2.3. X-ray powder diffraction

The hydrated and dehydrated forms of MIL-53(Ga)-FA were studied using a laboratory PANalytical X'PERT II powder diffractometer using a monochromatic Cu-$K_{\alpha 1}$ source (λ=1.5406 Å) with an operating voltage of 40 kV and a beam current of 40 mA. For the dehydrated phase, the sample was heated under secondary vacuum at 383 K for 8 hours and subsequently sealed in a glass capillary of diameter 0.5 mm. The patterns were collected for 2θ=5−100°. Full profile analysis (Le Bail intensity fitting together with refinement of lattice parameters) of individual X-ray powder diffraction (XRPD) patterns was performed using Jana 2006 software.[51]

2.4. High Pressure X-ray powder Diffraction

Angle-dispersive high-pressure XRPD data were collected at PSICHE beam line of the Synchrotron Soleil (Saint-Aubin, France) using a monochromatic beam (50×50 μm^2) with a wavelength of λ=0.37380 Å. The pressure was generated with a membrane diamond anvil cell (MDAC) using silicon oil AP100 (Aldrich) as the pressure-transmitting medium. The kinetic diameter of this silicon oil largely exceeds the window size of the MOF that ensures that this fluid does not enter the pores. The applied pressure was determined from the shift of the ruby R1 fluorescence line. XRPD measurements were also performed in-house (filtered Cu-$K_{\alpha 1}$, λ=1.5406Å) on the MOF powder samples that were pressed under a 13 mm IR-die at 6 tons corresponding to a mechanical pressure of 440 MPa. This experiment was performed in order to improve the resolution of the XRPD patterns of the contracted phase. Full profile analysis of this pressure-induced phase was performed with the same Jana 2006 software[51] that was used for indexing the hydrated and dehydrated phases.

2.5. Molecular Simulations

2.5.1. DFT structure optimization of MIL-53-FA frameworks.

The crystal structure of the dehydrated MIL-53(Ga)-FA was constructed starting from the framework model of the Al form we previously proposed.[42] This initial structure was further optimized at the DFT level with the Vienna *Ab initio* Simulation Package (VASP).[52-56] The PBE functional[57] was used and the van der Waals interactions were taken into account via semi-empirical dispersion corrections (DFT-D3 with Becke-Johnson damping).[58,59] A plane wave energy cut-off of 500 eV is employed together with a Gaussian smearing scheme with a smearing factor of 0.05 eV. The electronic (ionic) energy convergence is set to 10^{-8} eV (10^{-7} eV). A 6x2x2 *k*-point mesh is used with 6 *k*-points along the direction of the metal-oxide chain. These settings were found to be accurate for the analogue MIL-47(V^{IV}) material by Vanpoucke *et al*.[60] The MIL-53(Al)-FA was treated similarly in this work. The structures were optimized by constructing a local energy versus volume profile. As such the computational recipe of Vanpoucke *et al*.[60] was followed for the optimization of these structures with the construction of an equation-of-state (EOS) avoiding strong Pulay effects in flexible materials.[60] The cell shape and positions at each volume were fully relaxed. Finally, the profiles were fitted with a Vinet EOS[60,61] (see Supporting Information). The hessian of the large pore minimum for both materials was calculated with two displacements of 0.01 Å for every Cartesian degree of freedom. Afterward, the elastic constant tensor was calculated with the extended hessian approach.[60] The crystal structure of the hydrated MIL-53(Ga)-FA constructed starting from the framework model of the Al analogue, some of us previously proposed,[42] was further geometry optimized using the same computational strategy while fixing the cell parameters to that derived experimentally.

2.5.2. DFT Energy Profile as a Function of Volume

The *ab initio* energy profile as a function of volume at 0 K was computed for both empty aluminium and gallium fumarate based materials by means of a set of constrained geometry optimizations, in which the unit cell volume was kept fixed but the cell shape as well as the atomic positions are fully relaxed. Starting from the large pore phase, the volume was decreased until a metastable contracted phase was obtained. Subsequently, the structures around the metastable structure were optimized with a denser *k*-point mesh (6x2x6) and the Vinet EOS was used to obtain the minimum (see Supporting Information). The hessian was then calculated together with the elastic constant tensor.

3. Results and discussion

The hydrated form of MIL-53(Ga)-FA was considered initially, and its experimental XRPD pattern (see Figure 1) was indexed in a monoclinic space group $P2_1/c$, with a unit cell volume of ~1068.0(2) $Å^3$, slightly larger than the unit cell of the Al analogue (990 $Å^3$) (see Table 1). A plausible structural model of this hydrated structure was built using DFT calculations at fixed experimental unit cell parameters. This proposed structural model (Figure S11) is similar to the Al-analogue with however a more pronounced tilting of the organic linker which suggests a higher degree of flexibility of the Ga phase. Extensive hydrogen bonding interactions are observed between the water oxygens (Ow) and the μ_2-hydroxyl groups of the framework, and between the water protons and carboxylate oxygens (Figure S12). The Ow-H(μ_2-OH) distances are about 1.6 Å, indicating that the adsorbed water forms strong hydrogen bond with the MOF framework. Additionally, the water molecules form a 3D-hydrogen bond network with Ow-Hw distances ranging from 1.75 to 1.87 Å.

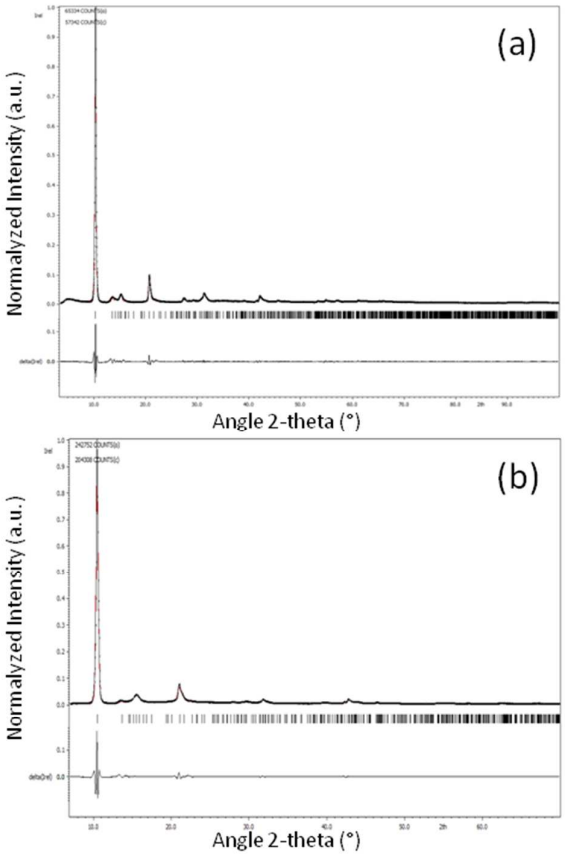

Fig. 1 *(a) Structure-independent refinement of the unit cell parameters for the hydrated phase of MIL-53(Ga)-FA, space group $P2_1/c$. a=7.159(1) Å, b=12.283(1) Å, c=14.461(2) Å, β=122.87(1)°, V=1068.0(2) $Å^3$. GoF=5.37 Rp=9.22 wRp=13.79. (b) Structure-independent refinement of the unit cell parameters for the hydrated phase of MIL-53(Al)-FA (see Table 1).*

Referring to our previous report on the mechanical behaviour of MIL-53(Al)-FA, the water molecules in the pores resist to the external pressure, and hence the solid does not undergo any structural change under applied pressure.[37] Since the hydrated MIL-53(Ga)-FA appears as isostructural to MIL-53(Al)-FA (Fig. 1(a) and (b)), mercury porosimetry and high-pressure XRPD experiments were not performed on the hydrated solid.

Table 1 *Experimental unit cell parameters of the hydrated, dehydrated and contracted phases of MIL-53(Al)-FA[37,42] as well as those of the hydrated and dehydrated phases of MIL53(Ga)-FA.*

	a (Å)	b (Å)	c (Å)	β (°)	V (Å^3)
MIL-53(Al)-FA					
Hydrated[42]	6.842(3)	12.088(3)	14.207(1)	122.55(7)	990.0(1)
Dehydrated[37]	7.022(3)	12.154(3)	14.745(5)	127.62(2)	998.0(1)
Contracted [37]	6.630	15.120	8.907	123.027	750.0
MIL-53(Ga)-FA					
Hydrated	7.159(1)	12.283(1)	14.461(2)	122.87(1)	1068.0(2)
Dehydrated	6.979(1)	12.458(4)	14.967(4)	128.48(2)	1018.8(6)

The dehydrated phase of MIL-53(Ga)-FA was then investigated. A structure-less refinement was successfully carried out for this structural form leading to a proposed unit cell with monoclinic symmetry (S.G. $P2_1/c$) and a volume of 1018.8 Å^3 (Figure 2) slightly higher than the Al analogue (volume of 998.0 Å^3). Based on the indexed cell parameters, a structural model was constructed and optimized with DFT by only relaxing the atomic positions. The resulting structural model of the dehydrated MIL-53(Ga)-FA is very close to that obtained earlier for the pristine dehydrated MIL-53(Al)-FA (Figure 2).[37] The dihedral angles for M-Oc-Cc-Cg_2 are similar, i.e. 176° and 170.1° for the Al and the Ga phases respectively (see Figure S8). The calculated powder pattern generated from the structural model was found to be in fair agreement with the experimental XRPD pattern (see Figure S13).

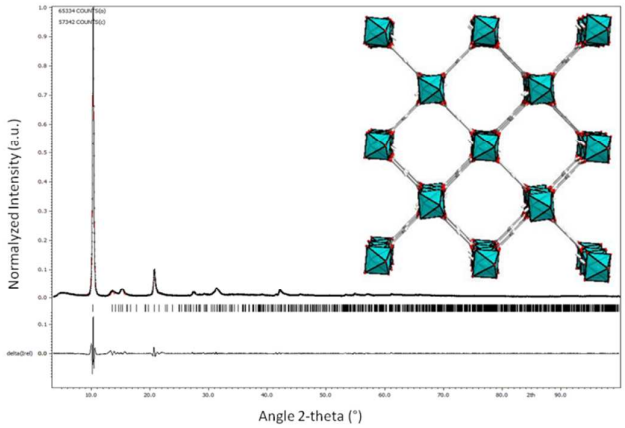

Fig. 2. *Structure-independent refinement of the unit cell parameters for the pristine phase of the dehydrated MIL-53(Ga)-FA , space group $P2_1/c$. a=6.979(1) Å, b=12.458(4) Å, c=14.967(5) Å, β=128.48(2)°, V=1018.8(6) Å^3. GoF=3.09, Rp=7.9, wRp=11.21. Inset: Polyhedral representation of the dehydrated MIL53(Ga)-FA. Ga octahedra: cyan, O: red and C in gray.*

The Hg porosimetry experiments on the dehydrated solid further indicated an increase in intruded volume until 20 MPa, which corresponds to compaction of the sample and intrusion of mercury between the particles (Figure 3).

A subsequent sharp increase in the intruded volume of Hg was observed above 85 MPa. Referring to our previous work on flexible microporous MOFs,[36,37,39] this can be ascribed to a structural transition (contraction) as Hg cannot penetrate into the micropores in the explored range of pressure. Similar pressure-induced behaviour has been observed for other flexible MOFs such as MIL-53(Cr)–BDC,[34] MIL-53(Al)–BDC[36] and MIL-47(V)–BDC[39]. The lower pressure of transition from the pristine to the contracted form with respect to the value evidenced for the isostructural Al-phase (P_{trans}=110 MPa) indicates a higher compressibility of the MIL-53(Ga)-FA.

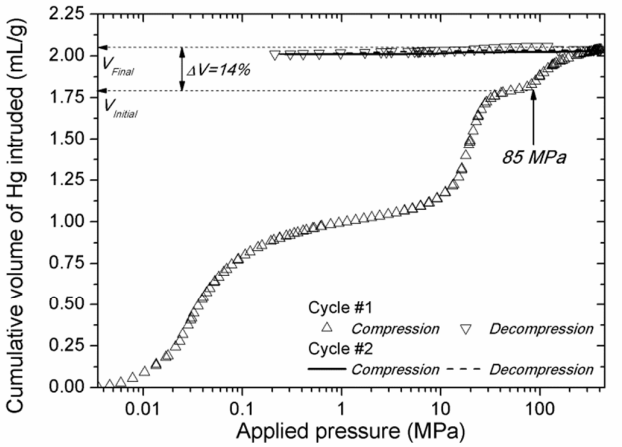

Fig. 3. *Cumulative volume of intruded mercury in two intrusion–extrusion cycles as a function of the applied pressure obtained for the activated MIL-53(Ga)–FA solid ($V_{Initial}$ and V_{Final} are the volumes of mercury intruded before and after the contraction of the solid respectively).*

The increase in the volume of intruded Hg measures 0.26 mL.g^{-1}. Starting with a unit cell volume of 1018.8 Å^3 for the dehydrated MIL-53(Ga)-FA structure, the volume of the contracted structure can be estimated to be ~875 Å^3 which remains higher than the volume for the Al contracted phase (750 Å^3). In contrast to MIL-53(Al)-FA, the structural transition is irreversible, which is noteworthy. Hence, the solid remains in its contracted pore form even after the pressure is released. Among the MIL-53-BDC frameworks, a similar behaviour has been observed previously in the case of MIL-53(Al)-BDC,[36] wherein an irreversible structural transition occurred at a lower pressure of 13-18 MPa. However, under similar conditions, the MIL-53(Cr)-BDC[34] analogue exhibits a reversible transition from the large pore form to a contracted pore form at a pressure of 55 MPa. High-pressure XRPD experiments were further performed on the dehydrated MIL-53(Ga)-FA in order to confirm the structural contraction of the structures expected from Hg porosimetry. These measurements reported in Figure 4 show that as the applied pressure increases, additional Bragg peaks appear which can be assigned to a new phase resulting from the pressure-induced contraction of the structure.

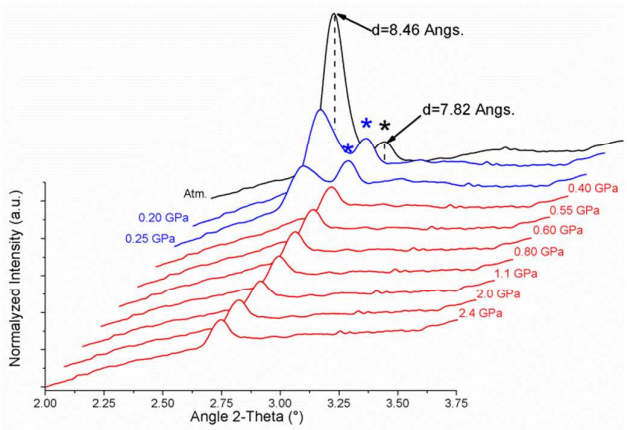

Fig. 4. *X-ray powder diffraction patterns of MIL-53(Ga)–FA as a function of the applied pressure (λ=0.37380 Å). The values of the applied pressure are in GPa. (* indicates the diffraction peaks assigned to the contracted pore form). The low-angle peaks at 2θ=2.51° (d=8.46 Å) and 2θ=2.74°(d=7.82 Å) correspond to the initial and contracted pore forms respectively.*

One can notice that a small amount of the contracted phase is still present at the initial stage of the experiment, arising due to a low transition pressure for the structural contraction, coupled with experimental limitations of the high-pressure cell. The low-angle peaks in the patterns recorded up to a pressure of 0.25 GPa correspond to d=8.46 Å (2θ=2.51°) and d=7.82 Å (2θ=2.74°) which can be assigned to the pristine and the contracted phases, respectively. Above 0.55 GPa, the experimental XRPD patterns correspond on the whole to this new phase, with the first peak at 2θ=2.74° (Figure 4).

Since Hg porosimetry revealed that the pressure-induced contraction of MIL-53(Ga)-FA is an irreversible process, a way to confirm this was to collect a XRPD pattern on the Ga-fumarate sample pressed in an IR-die (refer to Experimental Methods). The pattern shows peaks corresponding to the presence of both the initial and the contracted pore forms (Figure 5), the low-angle peaks at 2θ=10.46° (d=8.46 Å) and 2θ=11.32° (d=7.82 Å) corresponding to the same distances found in Figure 4. This clearly confirms the irreversibility of the structural transition. The poor experimental resolution of the high pressure XRPD patterns precluded an indexation of the contracted pore phase.

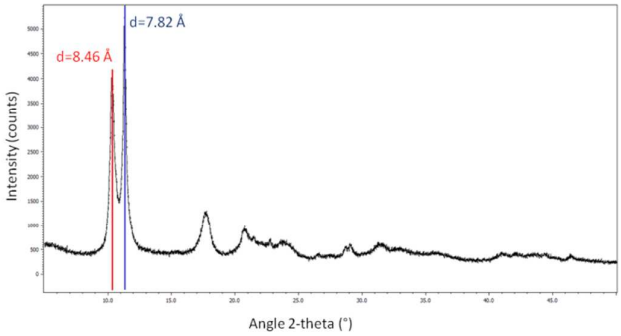

Fig. 5. *X-ray powder diffraction pattern (λ=1.5406Å) of dehydrated MIL53-Ga-FA pressed under a 13 mm IR-die up to a pressure of 440 MPa. The low-angle peaks at 2θ=10.46° (d=8.46 Å) and 2θ=11.32°(d=7.81 Å) correspond to the initial dehydrated form and contracted pore form respectively.*

Periodic DFT calculations were performed to further unravel the underlying features that are responsible for the different pressure-induced behaviour between the aluminium and gallium fumarate systems. The resulting energy profile as a function of volume E(V) is shown for both solids in Figure 6. The lattice parameters of the minima on the potential energy surface are summarized in Table 2.

The energy profile for both materials clearly illustrates the significant flexible behaviour of both materials. First, we focus our attention to Al-fumarate, for which the energy profile features a stable global minimum at a unit cell volume of 947 $Å^3$ (corresponding to the large pore or dehydrated phase, see Table 2) as well as a second metastable minimum at a smaller unit cell volume (corresponding to a contracted phase). The latter phase is barely bound as it is separated from the large pore phase by a very small barrier of less than 1 $kJ.mol^{-1}$ per unit cell. At finite temperature difference this minimum is expected to disappear due to entropic effects.[62] To motivate this statement, we computed that, within the normal mode approximation (NMA), the free energy of the contracted phase increases from 15 $kJ.mol^{-1}$ per unit cell at 0 K to 24.8 $kJ.mol^{-1}$ per unit cell at 300 K with respect to the large pore phase. As this increase of almost 10 $kJ.mol^{-1}$ is much larger than the barrier of 1 $kJ.mol^{-1}$ per unit cell, we expect the barrier to disappear at 300 K. More details on this NMA analysis can be found in the supporting information.

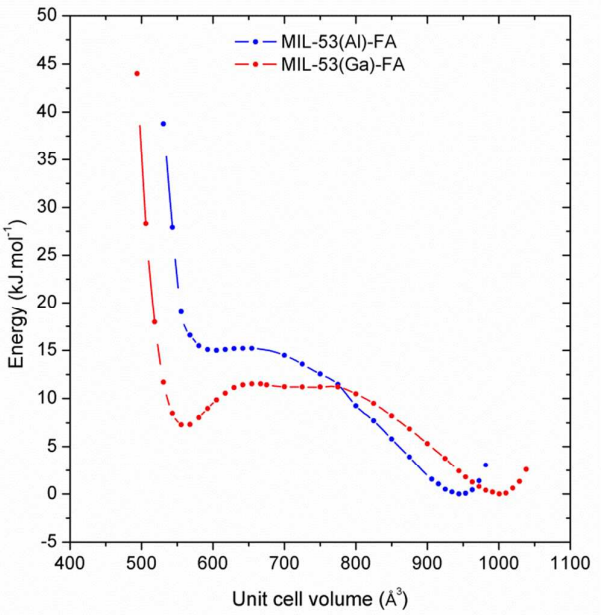

Fig. 6. *Ab initio energy profile as a function of the unit cell volume for Al- and Ga-fumarate at 0 K computed using constrained geometry optimizations in which only the unit cell volume is kept fixed.*

The Ga-fumarate profile is fundamentally different from the Al-variant, as now two well-defined stable structures are observed, one at a high volume of 1000 $Å^3$ (corresponding to a large pore or dehydrated phase) and one at a lower volume of 564 $Å^3$ (corresponding to a (fully) contracted pore phase). The

large pore form of Ga is associated with a unit cell volume (1000 Å^3) higher than the value simulated for the Al-analogue (947 Å^3). This prediction is in good agreement with the experimental sequence reported in Table 1. Furthermore, the large pore phase of Ga is 7 kJ.mol^{-1} per unit cell more stable than the contracted pore phase. Some care should be taken when considering absolute energy values, as they may vary upon using a different dispersion scheme,[62] although qualitatively the difference between the two materials bearing either aluminium or gallium is very clear. Due to the more strongly bound nature of the contracted phase with a higher barrier of almost 5 kJ.mol^{-1} per unit cell, this form can be expected to remain metastable at 300 K. Similarly, as it was done for the Al-fumarate, we computed that the free energy of the contracted phase increases from 7.2 kJ.mol^{-1} per unit cell at 0 K to 15.7 kJ.mol^{-1} per unit cell at 300 K with respect to the large pore phase. Since this increase of 8.5 kJ.mol^{-1} per unit cell is not significantly larger than the barrier at 0 K (5 kJ.mol^{-1}), we expect the barrier to remain at 300 K. As such, when pressure is applied and the structure contracts, the Ga-analogue will stay in the contracted phase after releasing the pressure. The presence of a well-defined energy minimum for the contracted phase resembles the experimentally observed trend of irreversible phase transition under applying an external pressure starting from the large pore phase.

An indicator of the higher structural rigidity of the Al-fumarate compared to the Ga-fumarate is the bulk modulus. This mechanical property is 4.1 GPa for Ga-fumarate obtained with a Vinet EOS fit[61], while the Al-fumarate has a bulk modulus of 5.0 GPa (see Supporting Information Figures S6-S9). This observation is consistent with a higher mechanical pressure required to induce the structural contraction of the Al-fumarate.

A further analysis of the elastic constants revealed that the anisotropy of the elastic properties of the materials under study was one order of magnitude lower than for the Al- and Ga-MIL-53-BDC (see Supporting information).[63,64]

Table 2 *Computed unit cell parameters of the large pore or dehydrated and the contracted pore forms of MIL-53(Al)-FA and MIL-53(Ga)-FA.*

	a (Å)	b (Å)	c (Å)	α (°)	β (°)	γ (°)	V (Å^3)
MIL-53(Al)-FA							
Dehydrated	6.688	13.437	13.760	90.0	130.0	90.0	947.0
Contracted	6.721	15.052	10.493	90.0	145.3	90.0	605.0
MIL-53(Ga)-FA							
Dehydrated	6.781	13.543	14.091	90.3	129.4	89.9	1000.4
Contracted	6.815	15.605	9.475	97.0	145.7	84.5	563.7

Further qualitative insights into the differences between the two materials may be obtained by deriving a pressure versus volume profile from a polynomial fit to the *ab initio* energy profile by taking the negative derivative of it (details of this procedure can be found in the supporting information). The resulting pressure profiles (see Figure S4) illustrate that the large pore to contracted phase transition pressure is higher for Al-fumarate than for Ga-fumarate, in line with the Hg-intrusion experiments. By means of the QuickFF procedure,[65,66] we traced the main source of difference in flexibility to the force constant of the M-O-C-C dihedral connecting the metal M(=Al/Ga) with the fumarate linker. This force constant is 10.4 kJ.mol^{-1} for Ga-fumarate and 19.9 kJ.mol^{-1} for Al-fumarate.

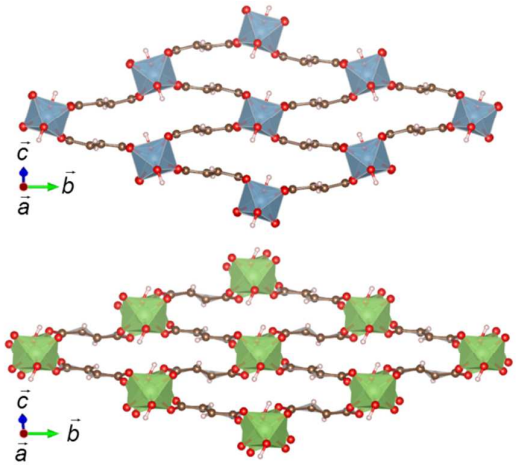

Fig. 7. *The DFT-structure models for the contracted pore form of the Al- (up) and Ga- (down) fumarate along the pore channel-direction.*

Finally, it can be noticed that the simulated contracted pore phases for Al- and Ga-fumarate slightly differ in unit cell parameters (see Table 2). While the DFT calculations reproduce well the cell dimensions of the large pore phases for both metals and the reversible/irreversible nature of the structural contraction of the Al- and Ga-fumarate respectively, it is noticeable that the contracted phases are predicted to be more closed for both metals than the experimental findings, the deviation being more pronounced for the Ga- material. The corresponding optimized crystal structures of the Al and Ga contracted phases are shown in Figure 7. While the contraction of the Al-fumarate is partly mediated by a decrease in the C-C-C-C dihedral angle, in the Ga-fumarate it is entirely driven by the change of the Ga-O-C-C dihedral angle (see Table S8 in Supporting Information).

Conclusions

In summary, the synthesis and characterization of MIL-53(Ga)-FA, the Ga analogue of the commercially available Al fumarate or MIL-53(Al)-FA porous MOF, has been for the first time carried out. The mechanical behaviour of the dehydrated MIL-53(Ga)-FA has been investigated using a combination of Hg porosimetry, high-pressure XRPD experiments and DFT calculations. These studies indicated that the structural transition from the initial to the contracted phase in this solid is irreversible, which is in contrast with what has been observed previously for MIL-53(Al)-FA. These experimental trends were further rationalized by constructing E(V) curves at 0 K. For the Ga-fumarate material two well-defined minima were present whereas for the aluminium version only a very shallow contracted phase minimum was obtained. At finite temperatures, it may thus be expected that the Ga-fumarate material undergoes an irreversible transition. Although experimental and computational methods did not lead to a consistent conclusion regarding the degree to which the material contracted, the experimental trends regarding (i) the higher pressure required to induce the contraction of phase for the Al-material owing to its higher degree of rigidity and (ii)

the reversibility/irreversibility of the pressure-induced transition were reproduced by the simulations. When considering mechanical-energy related applications, the irreversible structural contraction upon applied pressure reveals that MIL-53(Ga)-FA could be used in shock absorber applications, similar to that envisaged for MIL-53(Al)-BDC, and complementary to the application previously envisioned for MIL-53(Al)-FA, MIL-53(Cr)-BDC and MIL-47(V^{IV}) as nano-dampers. The results obtained indicate that MIL-53(Ga)-FA and related solids have potential for various real-world mechanical energy-related applications.

Acknowledgements

The authors would like to thank the French National Agency for Research ANR "MODS" (ANR-12-BS10-0005) for its financial support. We acknowledge the French national synchrotron radiation source "Synchrotron Soleil" (Saint-Aubin, France) for providing access to the PSICHE beam-line. VVS, JW and LV acknowledge the Research Board of Ghent University (BOF), the Fund for Scientific Research Flanders (FWO), BELSPO in the frame of IAP/7/05 and the European Union's Horizon 2020 research and innovation program (consolidator ERC grant agreement No 647755 – DYNPOR (2015-2020)). The computational resources and services used in this work were provided by VSC (Flemish Supercomputer Center), funded by the Hercules foundation and the Flemish Government – department EWI. G. M. thanks Institut Universitaire de France for its support.

Notes and references

1 H.-C Zhou, J. R. Long and O. M. Yaghi, *Chem. Rev.*, 2012, **112**, 673-674, and references therein.
2 H.-C. Zhou and S. Kitagawa, *Chem. Soc. Rev.*, 2014, **43**, 5415-5418, and references therein.
3 K. Sumida, D. L Rogow, J. A. Mason, T. M. McDonald, E. D. Bloch, Z. R Herm, T.-H. Bae and J. R. Long, *Chem. Rev.*, 2012, **112**, 724.
4 L. J. Murray, M. Dinca and J. R. Long, *Chem. Soc. Rev.*, 2009, **38**, 1294.
5 R. Vaidhyanathan, S. S. Iremonger, G. K. H. Shimizu, P. G. Boyd, S. Alavi and T. K. Woo, *Science*, 2010, **330**, 650.
6 Q. Yang, S. Vaesen, F. Ragon, A. D. Wiersum, D. Wu, A. Lago, T. Devic, C. Martineau, F. Taulelle, P. L. Llewellyn, H. Jobic, C. Zhong, C. Serre, G. De Weireld and G. Maurin, *Angew. Chem. Int. Ed.*, 2013, **52**, 10316.
7 7. H. Li, M. Eddaoudi, M. O'Keeffe and O. M. Yaghi, *Nature*, 1999, **402**, 276.
8 J. A. Mason, K. Sumida, Z. R. Herm, R. Krishna and J. R. Long, *Energy Environ. Sci.*, 2011, **4**, 3030.
9 S. Vaesen, V. Guillerm, Q. Yang, A. D.Wiersum, B. Marszalek, B. Gil, A.Vimont, M. Daturi, T. Devic, P. L. Llewellyn, C. Serre, G. Maurin and G. De Weireld, *Chem. Commun.*, 2013, **49**, 10082.
10 B. Van de Voorde, D. Damasceno Borges, F. Vermoortele, R. Wouters, B. Bozbiyik, J. Denayer, F. Taulelle, C. Martineau, C. Serre, G. Maurin and D. De Vos, *Chem. Sus. Chem*., 2015, **8**, 3159.
11 J.-R. Li, R. J. Kupplerand and H. -C. Zhou, *Chem. Soc. Rev.*, 2009, **38**, 1477.
12 A. Cadiau, J. S. Lee, D. Damasceno Borges, P. Fabry, T. Devic, M. T. Wharmby, C. Martineau, D. Foucher, F. Taulelle, C.-H. Jun, Y. K. Hwang, N. Stock, M. F. De Lange, F. Kapteijn, J. Gascon, G. Maurin, J. -S. Chang and C. Serre, *Adv. Mater.*, 2015, **27**, 4775.
13 P. Horcajada, R. Gref, T. Baati, P. K. Allan, G. Maurin, P. Couvreur, G. Férey, R. Morris and C. Serre, *Chem. Rev.*, 2012, **112**, 1232.
14 C. Orellana-Tavra, E. F. Baxter, T. Tian, T. D. Bennett, N. K. H. Slater, A. K. Cheetham and D. Fairen-Jimenez, *Chem. Commun.*, 2015, **51**, 13878.
15 T. Kajiwara, M. Higuchi, A. Yuasa, H. Higashimura and S. Kitagawa, *Chem. Commun.*, 2013, **49**, 10459.
16 D. Feng, W.–C. Chung, Z. Wei, Z.-Y. Gu, H.-L. Jiang, Y. -P. Chen, D. J. Darensbourg and H.-C. Zhou, *J. Am. Chem. Soc.*, 2013, **135**, 17105.
17 F. Vermoortele, M. Vandichel, B. Van de Voorde, R. Ameloot, M. Waroquier, V. Van Speybroeck and D. E. De Vos, *Angew. Chem. Int. Ed.*, 2012, **51**, 4887.
18 F. Vermoortele, B. Bueken, G. Le Bars, B. Van de Voorde, M. Vandichel, K. Houthoofd, A. Vimont, M. Daturi, M. Waroquier, V. Van Speybroeck, C. Kirschhock and D. E. De Vos, *J. Am. Chem. Soc.*, 2013, **135**, 11465.
19 L. Ma, O. R. Evans, B. M. Foxman and W. Lin, *Inorg. Chem.*, 1999, **38**, 5837.
20 M. D. Allendorf, C. A. Bauer, R. K. Bhakta and R. J. T. Houk, *Chem. Soc. Rev.*, **38**, 1330.
21 M. Wriedt, A. A. Yakovenko, G. J. Halder, A. V. Prosvirin, K. R. Dunbar and H. -C. Zhou, *J. Am. Chem. Soc.*, 2013, **135**, 4040.
22 M. Kurmoo, *Chem. Soc. Rev*., 2009, **38**, 1353.
23 D. Damasceno Borges, S. Devautour-Vinot, H. Jobic, J. Ollivier, F. Nouar, R. Semino, T. Devic, C. Serre, F. Paesani and G. Maurin, *Angew. Chem. Int. Ed.*, 2016, **55**, 3919.
24 P. Ramaswamy, N. E. Wong and G. K. H. Shimizu, *Chem. Soc. Rev.*, 2014, **43**, 5913.
25 A. Clearfield, *Dalton Trans.*, 2016, **45**, 4100.
26 K. W. Chapman, G. J. Halder and P. J. Chupas, *J. Am. Chem. Soc.*, 2008, **130**, 10524.
27 S. A. Moggach, T. D. Bennett and A. K. Cheetham, *Angew. Chem. Int. Ed.*, 2009, **48**, 7087.
28 J.-C. Tan, T. D. Bennett and A. K. Cheetham, *Proc. Nat. Acad. Sci. USA*, 2010, **107**, 9938.
29 T. D. Bennett, J.-C. Tan, S. A. Moggach, R. Galvelis, C. Mellot-Draznieks, B. A. Reisner, A. Thirumurugan, D. R. Allan and A. K. Cheetham, *Chem. Eur. J.*, 2010, **16**, 10684.
30 P. Serra-Crespo, A. Dikhtiarenko, E. Stavitski, J. Juan-Alcaniz, F. Kapteijn, F.-X. Coudert, J. Gascon, *Cryst. Eng. Comm.*, 2015, **17**, 276.
31 Y. H. Hu and L. Zhang, *Phys. Rev. B: Condens. Matter Mater. Phys.*, 2010, **81**, 174103.
32 S. M. J. Rogge, J. Wieme, L. Vanduyfhuys, S. Vandenbrande, G. Maurin, T. Verstraelen, M. Waroquier and V. Van Speybroeck, *Chem. Mater.*, 2016, **28**, 5721.
33 T. D. Bennett, P. Simoncic, S. A. Moggach, F. Gozzo, P. Macchi, D. A. Keen, J.–C. Tan and A. K. Cheetham, *Chem. Commun.*, 2011, **47**, 7983.
34 I. Beurroies, M. Boulhout, P. L. Llewellyn, B. Kuchta, G. Férey, C. Serre and R. Denoyel, *Angew. Chem. Int. Ed.*, 2010, **49**, 7526.
35 Q. Ma, Q. Yang, A. Ghoufi, K. Yang, M. Lei, G. Férey, C. Zhong and G. Maurin, *J. Mater. Chem. A*, 2014, **2**, 9691.
36 P. G. Yot, Z. Boudene, J. Macia, D. Granier, L. Vanduyfhuys, T. Verstraelen, V. Van Speybroeck, T. Devic, C. Serre, G. Férey, N. Stock and G. Maurin, *Chem. Commun.*, 2014, **50**, 9462.
37 P. G. Yot, L. Vanduyfhuys, E. Alvarez, J. Rodriguez, J.-P. Itié, P. Fabry, N. Guillou, T. Devic, I. Beurroies, P. L. Llewellyn, V. Van Speybroeck, C. Serre and G. Maurin, *Chem. Sci.*, 2016, **7**, 446.

38 P. G. Yot, K. Yang, V. Guillerm, F. Ragon, V. Dmitriev, P. Parisiades, E. Elkaïm, T. Devic, P. Horcajada, C. Serre, N. Stock, J. P. S. Mowat, P. A. Wright, G. Férey and G. Maurin, *Eur. J. Inorg. Chem.*, 2016, **27**, 4424.
39 P. G. Yot, Q. Ma, J. Haines, Q. Yang, A. Ghoufi, T. Devic, C. Serre, V. Dmitriev, G. Férey, C. Zhong and G. Maurin, *Chem. Sci.*, 2012, **3**, 1100.
40 C. L. Hobday, R. J. Marshall, C. F. Murphie, J. Sotelo, T. Richards, D. R. Allan, T. Düren, F.-X. Coudert, R. S. Forgan, C. A. Morrison, S. A. Moggach and T. D. Bennett, *Angew. Chem. Int. Ed.*, 2016, **55**, 2401.
41 P. G. Yot, K. Yang, F. Ragon, V. Dmitriev, T. Devic, P. Horcajada, C. Serre and G. Maurin, *Dalton Trans.*, 2016, **45**, 4283.
42 E. Alvarez, N. Guillou, C. Martineau, B. Bueken, B. van de Voorde, C. le Guillouzer, P. Fabry, F. Nouar, F. Taulelle, D. de Vos, J. -S. Chang, K. Ho Cho, N. Ramsahye, T. Devic, M. Daturi, G. Maurin and C. Serre, *Angew. Chem., Int. Ed.*, 2015, **54**, 3664.
43 F. Jeremias, D. Fröhlich, C. Janiak and S. K. Henninger, *RSC Adv.*, 2014, **4**, 24073.
44 C. Serre, F. Millange, C. Thouvenot, M. Nogues, G. Marsolier, D. Louer and G. Ferey, *J. Am. Chem. Soc.*, 2002, **124**, 13519.
45 A. S. Munn, A. J. Ramirez-Cuesta, F. Millange and R. I. Walton, *Chem. Phys.*, 2013, **427**, 30.
46 A. Boutin, M.-A. Springuel-Huet, A. Nossov, A. Gedeon, T. Loiseau, C. Volkringer, G. Férey, F.-X Coudert and A. H. Fuchs, *Angew Chem. Int. Ed.*, 2009, **48**, 8314.
47 A. Boutin, F.-X. Coudert, M.-A. Springuel-Huet, A. V. Neimark, G. Férey and A. H. Fuchs, *J. Phys. Chem. C*, 2010, **114**, 22237.
48 G. Weber, I. Bezverkhyy, J.-P. Bellat, A. Ballandras, G. Ortiz, G. Chaplais, J. Patarin, F.-X.Coudert, A. H. Fuchs and A. Boutin, *Micropor. Mesopor. Mat.*, 2016, **222**, 145.
49 R. S. Pillai, V. Benoit, A. Orsi, P. L. Llewellyn, P. A. Wright and G. Maurin, *J. Phys.Chem.C*, 2015, **119**, 23592.
50 A. S. Munn, R. S. Pillai, S. Biswas, N. Stock, G. Maurin and R. I. Walton, *Dalton Trans.*, 2016, **45**, 4162.
51 V. Petricek, M. Dusek and L. Palatinus, *Z. Kristallogr.* 2014, **229**, 345.
52 G. Kresse and J. Hafner, *Phys. Rev. B*, 1993, **47**, 558.
53 G. Kresse and J. Hafner, *Phys. Rev. B*, 1994, **49**, 14251.
54 G. Kresse and J. Furthmüller, *Comp. Mat. Sci.*, 1996, **6**, 15-50.
55 G. Kresse and J. Furthmüller, *Phys. Rev. B*, 1996, **54**, 11169.
56 G. Kresse and D. Joubert, *Phys. Rev. B*, 1999, **59**, 1758.
57 J. P. Perdew, K. Burke and M. Ernzerhof, *Phys. Rev. Lett.*, 1996, **77**, 3865.
58 S. Grimme, J. Antony, S. Ehrlich and H. Krieg, *J. Chem. Phys.*, 2010, **132**, 154104.
59 S. Grimme, S. Ehrlich and L. Goerigk, *J. Comput. Chem.*, 2011, **132**, 1456.
60 D. E. P. Vanpoucke, K. Lejaeghere, V. Van Speybroeck, M. Waroquier and A. Ghysels, *J. Phys. Chem. C*, 2015, **119**, 23752.
61 P. Vinet, J. Ferrante, J. H. Rose and J. R. Smith, *J. Geophys. Res.*, 1987, **92**, 9319.
62 A. M. Walker, B. Civalleri, B. Slater, C. Mellot-Draznieks, F. Corà, C. M. Zicovich-Wilson, G. Romàn-Perèz, J. M. Soler and J. D. Gale, *Angew. Chem. Int. Ed.*, 2010, **49**, 7501.
63 A. U. Ortiz, A. Boutin, A. H. Fuchs and F.-X. Coudert, *Phys. Rev. Lett.*, 2012, **109**, 195502.
64 A. U. Ortiz, A. Boutin, A. H. Fuchs and F.-X. Coudert, *J. Chem. Phys.*, 2013, **138**, 174703.
65 L. Vanduyfhuys, S. Vandenbrande, T. Verstraelen, R. Schmid, M. Waroquier and V. Van Speybroeck, *J. Comput. Chem.*, 2015, **36**, 1015
66 J. Wieme, L. Vanduyfhuys, S. M. J. Rogge, M. Waroquier and V. Van Speybroeck, *J. Phys. Chem. C*, 2016, **120**, 14934.

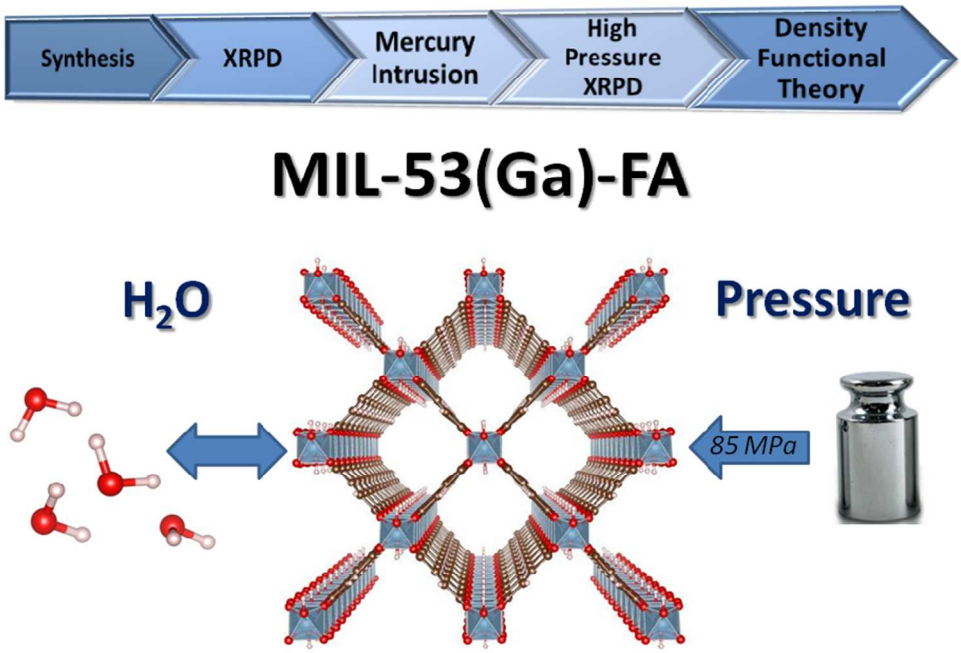

250x173mm (96 x 96 DPI)